An energy transfer accompanied by phonon absorption in ytterbium-doped yttrium aluminum perovskite for optical refrigeration

Nakayama, Y.

Harada, Y.

Kita, T.

Applied Physics Letters

An energy transfer accompanied by phonon absorption in ytterbium-doped yttrium aluminum perovskite for optical refrigeration

Cite as: Appl. Phys. Lett. **117**, 041104 (2020); https://doi.org/10.1063/5.0013213
Submitted: 08 May 2020 . Accepted: 14 July 2020 . Published Online: 28 July 2020

Y. Nakayama, Y. Harada, and T. Kita

AIP Publishing

Applied Physics Letters ARTICLE scitation.org/journal/apl

An energy transfer accompanied by phonon absorption in ytterbium-doped yttrium aluminum perovskite for optical refrigeration

Cite as: Appl. Phys. Lett. **117**, 041104 (2020); doi: 10.1063/5.0013213
Submitted: 8 May 2020 · Accepted: 14 July 2020 ·
Published Online: 28 July 2020

Y. Nakayama,[a] Y. Harada,[a] and T. Kita

AFFILIATIONS

Department of Electrical and Electronic Engineering, Graduate School of Engineering, Kobe University, Kobe 657-8501, Japan

[a]Authors to whom correspondence should be addressed: 179t250t@stu.kobe-u.ac.jp and y.harada@eedept.kobe-u.ac.jp

ABSTRACT

Yttrium aluminum perovskite (YAP) is a host material that can provide a strong emission from a rare-earth dopant and it has a lower phonon energy than yttrium aluminum garnet (YAG). Therefore, YAP is a promising material for optical refrigeration and radiation balanced laser. We measured the photoluminescence (PL) spectra of ytterbium (Yb)-doped YAP and compared them with those of Yb-doped YAG. The estimated ideal laser cooling efficiencies of Yb-doped YAP and Yb-doped YAG were comparable at 300 K. Based on the temperature-dependent anti-Stokes PL, we found that the laser cooling power of Yb-doped YAP at 470 K is 14.3 times higher than that at 200 K. This enhancement at higher temperatures is 3.2 times larger than that observed for Yb-doped YAG. We attributed the higher laser cooling power of Yb-doped YAP to a lower multi-phonon relaxation rate (and/or a higher energy transfer rate) and an antenna effect caused by the energy transfer from Yb ions that are located at the Y-site to Yb ions that are surrounded by an inhomogeneous alloy structure. The calculated small signal gain of (Yb:Y)AP is 3.5 times larger than that of (Yb:Y)AG. The larger small signal gain of (Yb:Y)AP arises from its strong absorbance and small Stark splitting width.

Heating of device parts near the cooling area is unavoidable for conventional electronic coolers. On the other hand, mechanical coolers usually introduce vibrations to the system. Laser cooling in solids can be used to avoid such problems, because here heat is carried away from the solid by the emission of photons.[1] The actual temperature drop (or net-cooling) of the solid under laser excitation has been observed in group II–VI semiconductors,[2] lead halide perovskites,[3] and rare-earth (RE)-doped materials.[4]

In the case of semiconductor materials, laser cooling can occur if electrons in the valence band absorb excitation light that is tuned to an energy within the Urbach tail, and the excited electrons or the excitons receive additional energy by phonon absorption. Then, if the emission of the anti-Stokes photoluminescence (PL) from the higher energy state occurs efficiently, the heat in the crystal lattice can be reduced. Theoretically, the excitonic resonances in the absorption and luminescence make a cooling of semiconductors down to cryogenic temperatures possible.[5] However, the high refractive indices of semiconductors lead to a reduced luminescence quantum yield. On the other hand, RE-doped materials usually have a lower refractive index and a weak photon (re-)absorption due to intra-orbital transitions. Additionally, a control of the quantum yield is possible by adjusting the doping concentration in these materials.[6] For example, it has been shown that an ultra-high-purity ytterbium (Yb)-doped crystal with a luminescence quantum yield near unity can be refrigerated to cryogenic temperatures.[7] In 2018, an all-solid-state cryocooler with an operating temperature of 135 K was demonstrated by using Yb-doped yttrium lithium fluoride (Yb:YLF).[8] Additionally, in 2019, a cooling grade Yb-doped yttrium aluminum garnet (Yb:YAG) realizes a radiation balanced laser (RBL) operation.[9]

To realize net cooling, a sufficiently low phonon energy E_p and a sufficiently small background absorption are required.[10,11] In particular, the cooling of RE-doped materials requires a low multi-phonon relaxation rate due to the low radiative rate of the f–f transition in the RE ion.[11] A low phonon energy is important, because the multi-phonon relaxation rate exponentially increases with the phonon energy of the phonons involved in the relaxation process. In fact, net cooling has often been observed in materials with low phonon energies.[4,10–20] Especially, Yb:YLF shows a significantly low maximum phonon energy of 440 cm^{-1}, and it was optically cooled to a cryogenic temperature below 100 K.[7,21]

Yb:YAG is also one of the better known cooling host materials.[12,18,22] The main motivations to use YAG are an enough low maximum phonon energy of $E_p = 106.1\,\text{meV}$ ($856\,\text{cm}^{-1}$), a good mechanical stability, a good chemical stability, and a high thermal conductivity.[6,18,22] Here, the maximum phonon energy is used to refer to the phonon mode with the highest wavenumber in the measured Raman spectrum at room temperature in the literature.[23,24] In addition, based on PL measurements, we reported that the ideal cooling efficiencies of Yb-doped YAG and Er-doped YAG are improved at high temperatures (above 300 K) due to an enhanced inhomogeneous anti-Stokes PL contribution.[25,26] An important result is that this "non-resonant" anti-Stokes PL showing the broadly distributed emission is the emission from RE ions surrounded by an inhomogeneous alloy structure. Here, the resonant anti-Stokes PL is defined as the emission originated by the intra-orbital *f*–*f* transitions between the ideal energy states of RE ions in the host crystal, which shows narrow PL peaks. A higher laser cooling efficiency in solids above 300 K may be useful for the cooling of light emitting diodes with a high output power[23] and RBL with a high output power creating heat under huge pump power.[9]

One other oxide material with properties that are similar to those of YAG is yttrium aluminum perovskite (YAP). It is one of the yttrium aluminate crystals that possess a phonon energy that is lower than that of YAG, i.e., $E_p = 76.9\,\text{meV}$ ($620\,\text{cm}^{-1}$) has been reported for YAP.[27] Using the above-mentioned phonon energies, the multi-phonon relaxation rates in Yb-doped YAG and Yb-doped YAP can be estimated by the following equation:[28]

$$W_{mp} = B\left(\frac{\exp\left(\frac{E_p}{k_B T}\right)}{\exp\left(\frac{E_p}{k_B T}\right) - 1}\right)^N \exp(-\alpha \Delta E), \quad (1)$$

where B is the spontaneous non-radiative decay rate, k_B is the Boltzmann constant, T is the absolute temperature, ΔE is the energy difference between two energy states, and $N = \Delta E/E_p$ is the number of phonons involved. The host-dependent parameter α is defined as $-\ln(\gamma)/E_p$, where γ is the electron–phonon coupling constant. It has been shown that $-\ln(\gamma)$ is usually almost constant ($\sim$3.5).[29] By assuming $B = 10^{12}\ \text{s}^{-1}$, $-\ln(\gamma) = 3.5$, $T = 300\,\text{K}$, and $\Delta E = 10{,}000\,\text{cm}^{-1}$, Eq. (1) predicts a multi-phonon relaxation rate of $7.09 \times 10^{-13}\ \text{s}^{-1}$ for Yb-doped YAP and $2.12 \times 10^{-6}\ \text{s}^{-1}$ for Yb-doped YAG. As the calculated multi-phonon relaxation rates are much smaller than the typical fluorescence decay rate W_f of Yb^{3+}, which is on the order of $10^3\ \text{s}^{-1}$, the radiative decay rate W_r is much larger than the multi-phonon relaxation rate. The much slower multi-phonon relaxation rate of Yb-doped YAP should result in a lower heat generation by non-radiative relaxation processes.

In this work, we measured the PL of Yb-doped YAP and analyzed the mean energy shift of the PL spectrum with respect to the excitation wavelength, the temperature dependence of the anti-Stokes PL intensity, and the small signal gain γ for RBL. We compared these data with those obtained from Yb-doped YAG. Our experimental results and analysis indicate that the stronger temperature-induced increase in the anti-Stokes PL intensity of Yb-doped YAP is caused by two factors: First, a lower multi-phonon relaxation rate (and/or a higher energy transfer rate). Second, an antenna effect caused by the energy transfer from Yb ions at sites with the symmetry of Y in yttrium aluminum oxide (i.e., Yb ions at the ideal Y-site) to Yb ions that are surrounded by an inhomogeneous alloy structure. Besides, the obtained results suggest the high output power of RBL by using (Yb:Y)AP due to its intrinsic material properties.

Hereafter, Yb-doped YAP is abbreviated as (Yb:Y)AP to clearly indicate at which site the Yb ion is nominally substituted. Accordingly, Yb-doped YAG is abbreviated as (Yb:Y)AG. The (Yb:Y)AG and (Yb:Y)AP ceramic samples for this work were fabricated by the solid-state reaction method. The Yb-doping concentration for two compared samples was fixed at a molar ratio of 0.1. Thus, the chemical formulas of (Yb:Y)AG and (Yb:Y)AP are $(Yb_{0.1}Y_{0.9})_3Al_5O_{12}$ and $(Yb_{0.1}Y_{0.9})AlO_3$, respectively. First, the high-purity (99.99%) raw materials (i.e., Yb_2O_3, Y_2O_3, and Al_2O_3) were mixed by ball milling. Then, a pressure of 200 MPa was applied to the mixed powder in a disc-shaped metal mold. After annealing in an electric furnace at 1000 °C for 10 h, the obtained thick ceramic sample was polished to remove contaminations at the surface. After surface polishing, the thickness of the ceramic sample is $\sim$2 mm. For the preparation of thin ceramic disks (thickness: approximately 100 μm), an additional mechanical polishing process was performed. The purity of the sample is not necessarily the same as that of starting materials because of segregation in the equilibrium crystal growth process in the solid-state-reaction method. For the PL measurements, a laser diode operating at 405 nm (3.06 eV) was used whose energy is larger than the energy gap between the ground state and the excited state of Yb^{3+}. According to the literature,[30] the excitation light of 405 nm is first absorbed by Yb^{2+} and the efficient energy transfer from Yb^{2+} to Yb^{3+} makes the emission at around 1 μm to originate from the *f*–*f* intra-orbital transition. This in-direct excitation process is useful to confirm the whole basic emission spectrum of Yb^{3+} at around 1 μm. The fluorescence was dispersed by a single monochromator (*F*-number: 3.88, grating with 600 l/mm and a blaze wavelength of 1000 nm) and detected by an InGaAs diode array. In the anti-Stokes PL and PL excitation (PLE) measurements, a supercontinuum light was passed through a double monochromator and the obtained monochromatic light (full width at half-maximum: 1.5 nm) was used to illuminate the ceramic samples.

Figure 1(a) shows the PL spectrum of (Yb:Y)AP at 300 K and the corresponding energy diagram for the resonant intra-orbital *f*–*f* transitions. The PL peak wavelengths of the resonant *f*–*f* transitions observed from the thin ceramic (blue curve) are 960 (E6 → E1), 979 (E5 → E1), 999 (E5 → E2), and 1038 nm (E5 → E4). The PL peaks at 974 and 1030 nm indicated by the asterisk (∗) are attributed to the signals from Yb^{3+} in YAG and yttrium aluminum monoclinic, respectively.[31,32] The thick ceramic [Fig. 1(a); dark blue curve] shows a broad PL spectrum, and the center wavelength of the signal is red-shifted due to strong re-absorption and re-emission processes. This strong absorption is detrimental in the case of resonant excitation: If a strong re-absorption of high energy anti-Stokes PL took place, the anti-Stokes PL quantum yield would be reduced and the low-energy Stokes PL signal would become stronger. The relaxation process responsible for generating the low-energy Stokes PL signal leads to internal heating. This re-absorption effect in (Yb:Y)AP is stronger than in (Yb:Y)AG, because of the higher absorbance. According to the literatures comparing the spectroscopic properties of (Yb:Y)AG and (Yb:Y)AP, the

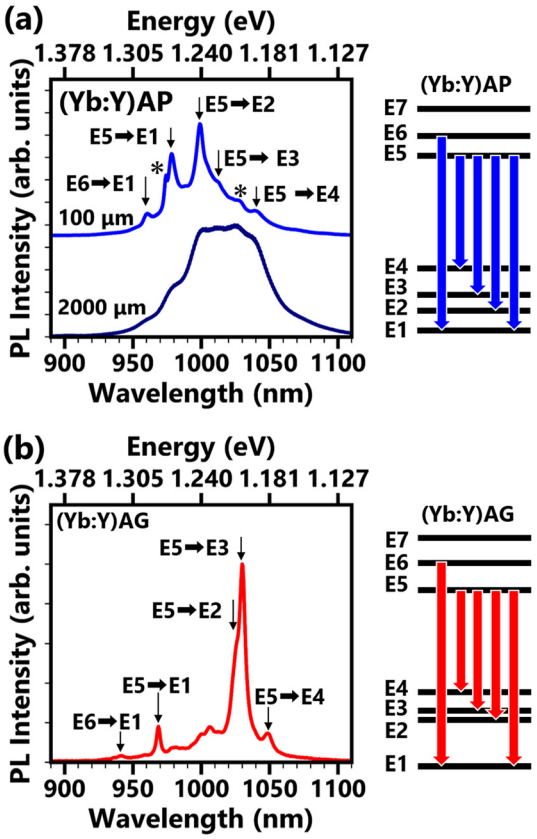

FIG. 1. PL spectra at 300 K and energy levels of (a) a thick and a thin (Y:Yb)AP ceramic and (b) a thin (Y:Yb)AG ceramic excited at 405 nm. The representative intra-orbital *f–f* transitions of Yb^{3+} in each host material are indicated in the diagrams on the right-hand side. The asterisks (∗) in (a) indicate the unexpected signals from Yb^{3+} ions in other yttrium aluminum oxides, such as YAG and yttrium aluminum monoclinic.

maximum absorption coefficient of the *f–f* intra-orbital transition in (Yb:Y)AP is 2–3 times larger than that of (Yb:Y)AG.[33,34] Additionally, as shown later, the ideal cooling efficiencies of (Yb:Y)AG and (Yb:Y)AP are almost the same. Therefore, the excitation power required to refrigerate (Yb:Y)AP should be at least ∼2 times smaller than that of (Yb:Y)AG. Figure 1(b) shows the sharp PL peaks of the thin (Yb:Y)AG ceramic. The assignment of the resonant transitions is as follows: 913 (E7 → E1), 940 (E6 → E1), 968 (E5 → E1), 1026 (E5 → E2), 1030 (E5 → E3), and 1048 nm (E5 → E4). The differences in the peak wavelengths and relative intensities of (Yb:Y)AG and (Yb:Y)AP arise from the different crystal fields around Yb^{3+} in each crystal structure. Additionally, the Yb ions surrounded by an inhomogeneous alloy structure result in the broadly distributed non-resonant signals in Figs. 1(a) and 1(b).

Figure 2 plots the excitation energy dependences of the mean energy shifts E_{shift} of the thin (Y:Yb)AG and (Y:Yb)AP ceramics (shown with triangles and diamonds, respectively) at 300 K. Here, the mean energy shift is defined as $E_{shift} = E_f - E_{exc}$, where E_f is the mean fluorescence energy and E_{exc} is the excitation energy in the PLE measurements. If the luminescence quantum yield of the material is 100%,

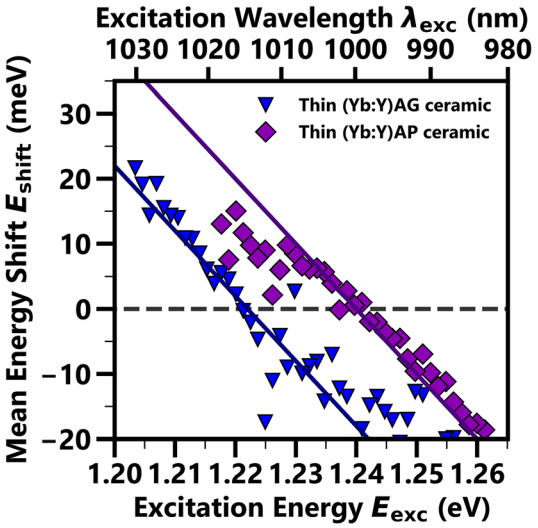

FIG. 2. The excitation energy dependence of the mean energy shift at 300 K. The results for (Y:Yb)AG and (Y:Yb)AP ceramics are shown with blue triangles and purple diamonds, respectively. The solid lines indicate the complement lines showing the excitation energy independent region of E_f, where E_{exc} < the optimum excitation energy.

the physical meaning of E_{shift} is the extracted energy per absorbed photon in the cooling process. $E_{shift} = 0$ is the point where the anti-Stokes PL component and the Stokes PL component are equal. In the region $E_{shift} > 0$, net cooling becomes possible because here the anti-Stokes PL component is dominant. The solid lines indicate a linear relationship showing the excitation independent region of E_f. The excitation energy dependence of the E_{shift} nicely obeys with the linear tendency below the optimum excitation wavelength confirmed by the relative cooling power.[25] The mean fluorescence energy E_f is constant in the excitation energy region where the considered contribution of the energy gap ΔE is small. The maximum mean energy shift of 17 meV in (Yb:Y)AP is comparable to the 22 meV in (Yb:Y)AG, indicating that the ideal cooling efficiency is almost independent of the maximum phonon energy of the host material. According to the Bose–Einstein distribution at 300 K (thermal energy: 25.7 meV or $\approx 207\ cm^{-1}$), the number of phonons with wavenumbers $>600\ cm^{-1}$ is more than 10 times smaller than the number of the low-energy optical phonons ($\approx 200\ cm^{-1}$). As a result, above the phonon energy of $600\ cm^{-1}$, the one-phonon absorption rate competes with that of the two-phonon process via absorption of low-energy phonons. We computed the phonon absorption rate based on the single-frequency model by Auzel.[35] Therefore, the contribution of the maximum-energy phonons to the anti-Stokes process is small at room temperature.

The temperature-dependent phonon absorption process in each material provides insights into the possibilities for optical refrigeration at high temperatures. Figure 3(a) shows the temperature dependences of the integrated anti-Stokes PL intensities. The temperature was changed from 200 to 470 K, and the PL intensities were normalized at 200 K. The red circles and blue triangles indicate the values obtained by the optimum excitation of the E4–E6-transitions in (Yb:Y)AP and the E3–E5-transitions in (Yb:Y)AG, respectively. The optimum

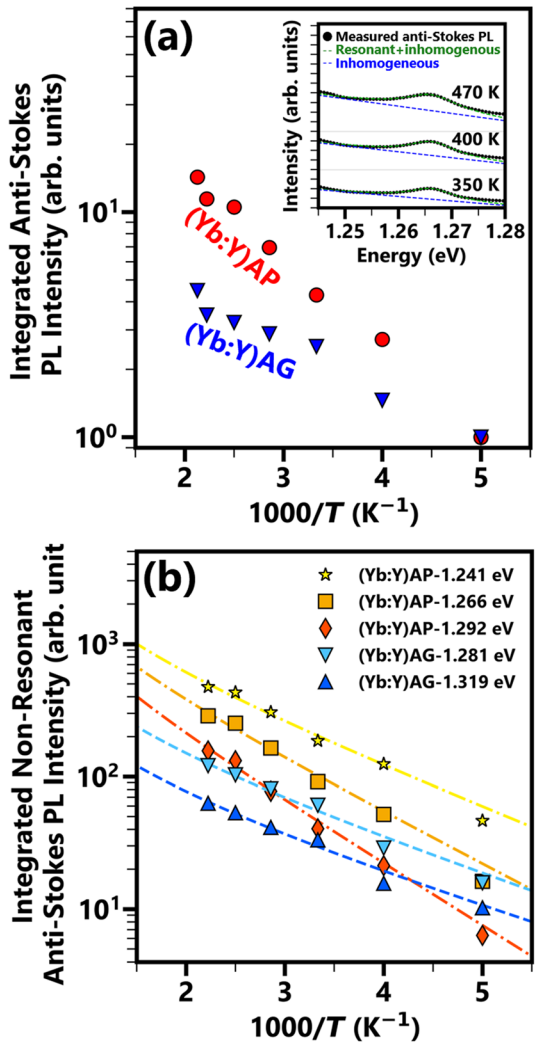

FIG. 3. (a) The temperature dependences of the integrated anti-Stokes PL intensities of (Yb:Y)AG and (Yb:Y)AP. The anti-Stokes PL spectra were measured under a resonant excitation at 1030 nm (1.204 eV; E3 → E5) for (Yb:Y)AG and 1018 nm (1.218 eV; E4 → E6) for (Yb:Y)AP. The inset shows the anti-Stokes PL spectra of (Yb:Y)AP and the fitting curves used to identify the resonant and inhomogeneous anti-Stokes PL components. (b) The temperature dependences of the integrated inhomogeneous anti-Stokes PL peak intensities. The dashed lines indicate the fitting results obtained by using Eq. (2).

excitation wavelengths in both materials were confirmed by the relative cooling power as the function of the excitation wavelength. The inset in Fig. 3(a) shows a typical temperature dependence of the anti-Stokes PL spectrum of (Yb:Y)AP, including the fitting curves. Here, Lorentzian and monotonically varying functions were assumed to evaluate the resonant and inhomogeneous anti-Stokes PL components, respectively,. According to Fig. 3(a), the integrated anti-Stokes PL intensity of (Yb:Y)AP at 470 K is 14.3 times larger than that at 200 K. This increase is a result of the enhanced inhomogeneous anti-Stokes PL at higher temperatures. On the other hand, the integrated anti-Stokes PL intensity of (Yb:Y)AG at 470 K is only 4.5 times larger than that at 200 K. The inhomogeneous anti-Stokes PL intensities of (Yb:Y)AP and (Yb:Y)AG exhibit an exponential increase as the temperature increases, while the resonant anti-Stokes PL intensity saturates, as shown in the inset of Fig. 3(a) and the literature.[25] The difference of two excitation conditions does not affect our conclusion. We experimentally confirmed the difference in the excitation wavelength. Even when the excitation wavelength is longer than the optimal excitation wavelength for (Yb:Y)AG, the integrated PL intensity of (Yb:Y)AP shows the large enhancement with increasing the temperature as same as that under the 1018 nm excitation.

Figure 3(b) provides the temperature dependences of the integrated inhomogeneous anti-Stokes PL intensities. The yellow stars, orange squares, and red diamonds are used to plot the peak intensities of (Yb:Y)AP at 1.292, 1.266, and 1.241 eV ± 7 meV, respectively. The light blue downward triangles and the blue upward triangles are used to plot the peaks of (Yb:Y)AG at 1.319 and 1.281 eV ± 7 meV, respectively. The inclination of the data for (Yb:Y)AP is significantly larger. The curves in Fig. 3(b) are the fitting results obtained using the Bose–Einstein function,

$$f_{BE}(T) = \frac{A}{e^{\frac{\varepsilon}{k_B T}} - 1}, \tag{2}$$

where A is a constant value that is proportional to the mean energy transfer rate W_{mET}, and ε is the mean of the absorbed phonon energy. There are three possible processes for the excited electron: radiative relaxation, multi-phonon relaxation, and energy transfer.[36] The inhomogeneous anti-Stokes PL is generated through the energy transfer process from the ideally doped Yb ion to inhomogeneously doped Yb ion. Then, the mean energy transfer rate W_{mET} can be written as

$$A \propto W_{\mathrm{mET}} = \frac{W_{\mathrm{ET}}}{W_{\mathrm{r}} + W_{\mathrm{mp}} + W_{\mathrm{ET}}}. \tag{3}$$

Here, W_{r} is the radiative decay rate, W_{mp} is the multi-phonon relaxation rate, and W_{ET} is the energy transfer rate from Yb ions at the Y-site to Yb ions surrounded by an inhomogeneous alloy structure. The phonon absorption process simultaneously occurs with this energy transfer.

The A and the ε for our two samples were determined by a least squares fitting procedure. The values obtained for the inhomogeneous anti-Stokes PL at 1.292 eV ± 7 meV in (Yb:Y)AP are $A = 1.62 \times 10^3$ and $\varepsilon = 92.6$ meV. Those for the inhomogeneous anti-Stokes PL at 1.319 eV ± 7 meV in (Yb:Y)AG are $A = 1.52 \times 10^2$ and $\varepsilon = 46.9$ meV. A small W_{mp} and a large W_{ET} lead to a large A according to Eq. (3) and the assumptions that W_{r} takes a typical value of Yb^{3+} $\sim 1 \times 10^3$ s^{-1}. Thus, the larger A in (Yb:Y)AP indicates a lower multi-phonon relaxation rate and/or a higher energy transfer rate than in (Yb:Y)AG. The larger ε in (Yb:Y)AP indicates a difference in the energy structure of the Yb ions located within an inhomogeneous alloy. These Yb ions exhibit a broadly distributed energy structure in the macroscopic view, but each ion has discrete energy levels. Therefore, the phonon-assisted energy transfer process is possible, and the large energy gap between the energy levels of Yb ions at the Y-site and Yb ions within an inhomogeneous alloy in (Yb:Y)AP results in the large ε. As mentioned above, in Fig. 3(b), the inclination of the inhomogeneous anti-Stokes PL of (Yb:Y)AP is steeper than that of (Yb:Y)AG. The large ε of (Yb:Y)AP can explain these significantly enhanced inhomogeneous anti-Stokes PL

intensities at elevated temperatures. As a result of the low multi-phonon relaxation rate (and/or the high energy transfer rate) and the high mean of the absorbed phonon energy, (Yb:Y)AP is a promising oxide laser-cooling material for high operating temperatures above 300 K.

The presented results of (Yb:Y)AP above suggest the capability for RBL. We characterized (Yb:Y)AG and (Yb:Y)AP as an RBL medium by the gain γ:[9] we used the reciprocal relationship[37] to obtain the absorption spectra from the emission spectra in Fig. 1 and referred the typical intrinsic parameters of (Yb:Y)AG and (Yb:Y)AP (energy structure,[38,39] fluorescence lifetime,[31,39] crystal structure[40]).

The selected excitation wavelengths λ_P of 1030 nm for (Yb:Y)AG and of 1018 nm for (Yb:Y)AP are the optimum excitation wavelengths in each material. The maximum gain of 0.27 cm^{-1} in (Yb:Y)AP at 1041.3 nm is 3.5 times larger than that of 0.078 cm^{-1} in (Yb:Y)AG at 1049.7 nm. The larger gain in (Yb:Y)AP compared with that in (Yb:Y)AG arises from its strong absorption and the energy structure with small Stark splitting energy. The absorption coefficients of (Yb:Y)AG and (Yb:Y)AP at λ_L are 0.074 cm^{-1} and 0.19 cm^{-1}, respectively, and the parameter β_P/β_L of (Yb:Y)AG and (Yb:Y)AP at λ_L are 2.2 and 2.9, respectively. Therefore, (Yb:Y)AP can be considered as the RBL medium with a higher output power than (Yb:Y)AG.

In summary, we have discussed the PL spectra of (Yb:Y)AP, the mean energy shift, the anti-Stokes PL temperature dependence, and the small signal gain to understand its potential for optical refrigeration and RBL. The red-shifted PL spectrum of the thick (Yb:Y)AP ceramic was explained with a strong absorbance. We suppressed the re-absorption effect by decreasing the thickness. The thin (Yb:Y)AP sample had a mean energy shift of 17 meV, which is comparable to that of (Yb:Y)AG. The temperature dependence of the anti-Stokes PL indicated a low multi-phonon relaxation rate (and/or a high energy transfer rate) and a large mean of the absorbed phonon energy in (Yb:Y)AP. We have explained that this phonon absorption simultaneously occurs with the energy transfer from an Yb ion at the Y-site to an Yb ion within an inhomogeneous alloy. We have compared the enhancements in the integrated anti-Stokes intensities of (Yb:Y)AP and (Yb:Y)AG that were observed when the temperature was increased from 200 to 470 K. The 3.2 times stronger enhancement in (Yb:Y)AP indicates not only a high laser-cooling power of (Yb:Y)AP but also the capability for RBL above 300 K. The calculated small signal gain γ of (Yb:Y)AP is 3.5 times larger than that of (Yb:Y)AG. The large γ of (Yb:Y)AP arises from its strong absorbance and small Stark splitting width.

DATA AVAILABILITY

The data that support the findings of this study are available from the corresponding author upon reasonable request.

REFERENCES

[1]B. C. Edwards, M. I. Buchwald, R. I. Epstein, T. R. Gosnell, and C. E. Mungan, in *Proceedings of the 9th Annual AIAA/USU Conference on Small Satellites*, edited by F. Redd (Utah State University, Logan, 1995), pp. 1–9.
[2]J. Zhang, D. Li, R. Chen, and Q. Xiong, Nature **493**, 504 (2013).
[3]S. T. Ha, C. Shen, J. Zhang, and Q. Xiong, Nat. Photonics **10**, 115 (2016).
[4]R. I. Epstein, M. I. Buchwald, B. C. Edwards, T. R. Gosnell, and C. E. Mungan, Nature **377**, 500 (1995).
[5]G. Rupper, N. H. Kwong, and R. Binder, Phys. Rev. Lett. **97**, 117401 (2006).
[6]G. Nemova and R. Kashyap, J. Lumin. **164**, 99 (2015).
[7]S. D. Melgaard, A. R. Albrecht, M. P. Hehlen, and M. Sheik-Bahae, Sci. Rep. **6**, 20380 (2016).
[8]M. P. Hehlen, J. Meng, A. R. Albrecht, E. R. Lee, A. Gragossian, S. P. Love, C. E. Hamilton, R. I. Epstein, and M. Sheik-Bahae, Light Sci. Appl. **7**, 1 (2018).
[9]Z. Yang, J. Meng, A. R. Albrecht, and M. Sheik-Bahae, Opt. Express **27**, 1392 (2019).
[10]T. Kushida and J. E. Geusic, Phys. Rev. Lett. **21**, 1172 (1968).
[11]M. P. Hehlen, Proc. SPIE **7228**, 72280E (2009).
[12]R. I. Epstein, J. J. Brown, B. C. Edwards, and A. Gibbs, J. Appl. Phys. **90**, 4815 (2001).
[13]J. Thiede, J. Distel, S. R. Greenfield, and R. I. Epstein, Appl. Phys. Lett. **86**, 154107 (2005).
[14]D. V. Seletskiy, S. D. Melgaard, S. Bigotta, A. D. Lieto, M. Tonelli, and M. Sheik-Bahae, Nat. Photonics **4**, 161 (2010).
[15]M. Malinowski, Opt. Express **16**, 873 (2011).
[16]S. D. Melgaard, "Cryogenic optical refrigeration: Laser cooling of solids below 123 K" Doctoral dissertation (The University of New Mexico, 2013).
[17]S. Melgaard, D. Seletskiy, V. Polyak, Y. Asmerom, and M. Sheik-Bahae, Opt. Express **22**, 7756 (2014).
[18]E. S. D. L. Filho, G. Nemova, S. Loranger, and R. Kashyap, Opt. Express **21**, 24711 (2013).
[19]A. Volpi, A. D. Lieto, and M. Tonelli, Opt. Express **23**, 8216 (2015).
[20]S. Rostami, A. R. Albrecht, A. Volpi, and M. Sheik-Bahae, Photonics Res. **7**, 445 (2019).
[21]X. X. Zhang, A. Schulte, and B. H. T. Chai, Solid State Commun. **89**, 181 (1994).
[22]G. Nemova and R. Kashyap, J. Opt. Soc. Am. B **31**, 340 (2014).
[23]Y. F. Chen, P. K. Lim, S. J. Lim, Y. J. Yang, L. J. Hu, H. P. Chiang, and W. S. Tse, J. Raman Spectrosc. **34**, 882 (2003).
[24]J. Arvanitidis, K. Papagelis, D. Christofilos, H. Kimura, G. A. Kourouklis, and S. Ves, Phys. Status Solidi Basic Res. **241**, 3149 (2004).
[25]Y. Nakayama, Y. Harada, and T. Kita, Opt. Express **27**, 34961 (2019).
[26]Y. Nakayama, Y. Harada, and T. Kita, Proc. SPIE **11298**, 112980B (2020).
[27]J. Suda, O. Kamishima, K. Hamaoka, I. Matsubara, T. Hattori, and T. Sato, J. Phys. Soc. Jpn. **72**, 1418 (2003).
[28]W. Miniscalco, in *Rare-Earth Doped Fiber Lasers and Amplifiers*, edited by M. J. F. Digonnet, 2nd ed. (Mrcel Dekker, Inc., 2001), pp. 29–33.
[29]J. M. F. van Dijk and M. F. H. Schuurmans, J. Chem. Phys. **78**, 5317 (1983).
[30]S. Rydberg and M. Engholm, J. Appl. Phys. **113**, 223510 (2013).
[31]F. D. Patel, E. C. Honea, J. Speth, S. A. Payne, R. Hutcheson, and R. Equall, IEEE J. Quantum Electron. **37**, 135 (2001).
[32]L. Lipińska, A. Rzepka, R. Ryba-Romanowski, D. Klimm, S. Ganschow, and R. Diduszko, Cryst. Res. Technol. **44**, 146 (2009).
[33]X. Zeng, G. Zhao, X. Xu, H. Li, J. Xu, Z. Zhao, X. He, H. Pang, M. Jie, and C. Yan, J. Cryst. Growth **274**, 106 (2005).
[34]X. Wang, X. Xu, Z. Zhao, B. Jiang, J. Xu, G. Zhao, P. Deng, G. Bourdet, and J. C. Chanteloup, Opt. Mater. **29**, 1662 (2007).
[35]F. Auzel, Phys. Rev. B **13**, 2809 (1976).
[36]H. Toratani, T. Izumitani, and H. Kuroda, J. Non. Cryst. Solids **52**, 303 (1982).
[37]R. M. Martin and R. S. Quimby, J. Opt. Soc. Am. B **23**, 1770 (2006).
[38]R. J. Beach, Opt. Commun. **123**, 385 (1996).
[39]G. Boulon, Y. Guyot, H. Canibano, S. Hraiech, and A. Yoshikawa, J. Opt. Soc. Am. B **25**, 884 (2008).
[40]X. Zhan, Z. Li, B. Liu, J. Wang, Y. Zhou, and Z. Hu, J. Am. Ceram. Soc. **95**, 1429 (2012).